Editors' Suggestion

Space-time electron wave packets with tunable skyrmion textures

Sharoz Schezwen
School of Electrical and Electronics Engineering, Nanyang Technological University, Singapore

Yijie Shen*
Centre of Disruptive Photonics Technologies, School of Physical and Mathematical Sciences, Singapore and School of Electrical and Electronics Engineering, Nanyang Technological University, Singapore

(Received 2 July 2026; accepted 9 September 2026; published 7 October 2026)

Space-time wave packets (STWPs) have enabled numerous nontrivial properties, such as tunable group velocities, nondiffraction, and nonlocal spin textures in optical fields. However, they have not been properly studied in matter waves. Here, we investigate free-electron STWPs, which are propagation-invariant and group-velocity-tunable matter wave packets, constructed by constraining the spatiotemporal spectrum of the electron wavefunction in momentum space. Due to the unique dispersion of free electrons, the electron STWP can carry two different topologies and host both meron and skyrmion topological textures in momentum space. We demonstrate the topological phase transitions and tunable skyrmion numbers by spectral geometry tuning. We also show the topologically robust propagation of the electron pulses and corresponding real-space skyrmionic expectation value textures encoded within each single electron wavefunction. Our results open a platform for topological free-electron wave packets uses in sensing and information transfer.

DOI: 10.1103/pnvl-7bx7

I. INTRODUCTION

Structured free-electron waves have emerged as a reliable and powerful platform to control quantum matter waves, enabling the creation of electron vortex beams carrying angular momentum [1–4], to shaped electron wave packets used for microscopy and spectroscopy [5–7]. Yet single free-electron wave packets remain fundamentally limited by issues such as the diffractive spreading and dispersion, and temporal walk-off that limit the interaction lengths in free-electron-photon interactions; persistent bottlenecks in electron optics applications [8–10]. Beyond this, a free electron has an intrinsic spin degree of freedom, fundamentally limiting the possibility of creating spin textures for single electrons [11]. Such spin textures may provide fast spin filters for measuring material spin textures from the Hund's exchange term in the interaction Hamiltonian [12,13] (see Sec. F of the Supplemental Material [14]), without the need for complex vector reconstruction or sample tilting.

Recently, space-time wave packets (STWPs) are an emerging class of structured waves with a correlated space and time degrees of freedom, which give the waves a well-defined and tunable group velocity and great resistance against ordinary diffraction and dispersion [15–32]. An optical

*Contact author: yijie.shen@ntu.edu.sg

Published by the American Physical Society under the terms of the Creative Commons Attribution 4.0 International license. Further distribution of this work must maintain attribution to the author(s) and the published article's title, journal citation, and DOI.

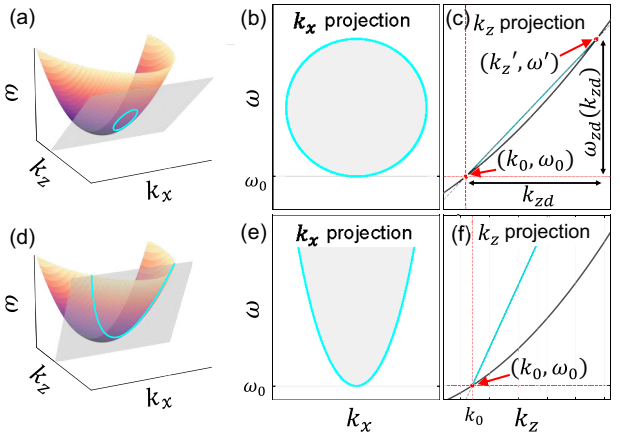


FIG. 1. (a) The construction of momentum space skyrmion uses a closed spectral loop in (b) $k_x - \omega$ space. (c) The intersection of the spectral plane and the dispersion surface gives the lowest point (k_0, ω_0) called the carrier, and the point (k_z', ω'). The difference between them is k_{zd}. When ω' is the maximum allowed constituent electron plane wave energy, we write the point as $(k_{z\max}, \omega_{\max})$ in text. (d)–(f) Merons can be obtained from an intersection that produces a parabolic projection in the $k_x - \omega$ plane instead.

STWP was also shown to carry a nondiffracting meron by using a metasurface to imprint a polarization texture in momentum space [33], while related momentum space merons have also been realized through photonic crystal slabs [34,35]. The merons are a half skyrmion, topologically nontrivial spin textures originally introduced in nuclear physics, which have since been obtained in other fields [36–46]. The key feature of a skyrmionic texture is the topological robustness, making it attractive for robust transport and information encoding [47–49]. In optical STWP, the fundamental structure of the light cone makes the meron the only naturally available topological structure. However, nonrelativistic free electrons obey a quadratic dispersion relation ($\omega = \hbar k^2/2m$) [see Fig. 1(a)] on the dispersion surface. This allows a free-electron STWP to be nondiffracting and nondispersive, have tunable group velocities, and to host full or half skyrmionic topologies in momentum space and the corresponding real-space wavefunction. Such realization gives an entirely new degree of freedom for free electrons.

In this paper, we show this construction of nonrelativistic free-electron STWP by engineering the spatiotemporal spectrum on the quadratic dispersion relation. We show that despite being propagation invariant, such construction also supports momentum space skyrmions and merons, and we further derive the analytical topological phase transition between them. In real space, we show the existence of propagation-invariant skyrmion and meron textures in the local spin expectation value (SEV) that remain robust upon extended propagation distances. This establishes a route toward topologically structured electron wave packets whose real-space topologies are transported unchanged in free space, for use in sensing and information transfer.

II. RESULTS

To construct an electron STWP, the free-electron dispersion relation is given by the solution to the Schrödinger equation in a closed system, written as $\omega = \hbar k^2/2m$, where k^2 and m are the momentum and the mass of the elementary electron. Throughout this paper, both $\hbar$ and m are taken to be 1 for the analytical calculations. A spectral constraint in the form of a plane [$\omega = \omega_0 + \tan\theta(k_z - k_0)$] intersects the dispersion surface at an angle θ, giving a well-defined group velocity of the electron wave packet [Fig. 1(a)]. The intersection curve, called the spectral support curve, can be projected onto the $k_x - \omega$ plane [Fig. 1(b)], which shares at least one point (k_0, ω_0) with the spectral plane. We

call this lowest frequency ω_0 the carrier frequency, as seen in the $k_z - \omega$ plane [Fig. 1(c)]. Tuning the parameters k_0 and θ (the tilt of the spectral plane) gives different spectral projections onto the plane $k_x - \omega$ and $k_z - \omega$ [Figs. 1(d)–1(f)]. In this paper, we focus on the superluminal electrons with group velocities above the carrier group velocity at (k_0, ω_0).

These projections form the energy-momentum relations that the electron plane waves should possess to form a single electron STWP. Upon introducing the dimension k_y, the curve in Figs. 1(b) and 1(e) is revolved into a three-dimensional (3D) surface in momentum space. The different topologies of the three-dimensional surfaces, either closed or open, are used to form momentum space skyrmions and fractional skyrmions, respectively. This is due to the momentum space surface covering a full Bloch sphere, or a portion of the Bloch sphere. This will be detailed more below. We first give an analytic description of the range where momentum space merons and skyrmions can be hosted in an electron STWP based on the three-dimensional topology of the spectral surface and for a given maximum electron energy with frequency $\omega_{\max}$.

To investigate the topology, the value of the carrier wave number and the group velocity was used as free parameters. First, by imposing a condition where the spectral plane intersects the dispersion surface at exactly the carrier frequency, the lowest group velocity where the electron wave packets has to possess to get a closed momentum space surface is obtained. This is equivalent to the gradient of the dispersion surface $\partial\omega/\partial k_z$ at the point (k_0, ω_0). The group velocity has to satisfy Eq. (1) for the electron wave packet to host a momentum space skyrmion,

$$v_g > \frac{\hbar k_0}{m}. \tag{1}$$

At the same time, there is an upper limit after which only open momentum space surfaces can be obtained, and therefore only merons can be hosted. The analytical starting point depends on a given maximum electron energy making up the wave packet. We note that the largest group velocity that can host a skyrmion is when the spectral plane cuts the dispersion surface at exactly k_0 and $k_{z\max}$, where $k_{z\max}$ is the maximum value of the longitudinal wave number where the spectral plane can intersect the dispersion surface [Fig. 1(c) and the corresponding figure caption, $k_{z\max} = 10$ in Fig. 2]. This directly leads to the constraint in Eq. (2). Both group velocity constraints for merons and skyrmions are visualized in Fig. 2(a),

$$v_g > \frac{\hbar\left(k_{z\max}^2 - k_0^2\right)}{2m\left(k_{z\max} - k_0\right)}. \tag{2}$$

Within the region that can host skyrmions, the closed three-dimensional surface spanned by (k_x, k_y, ω) also has a size dependence on the group velocity and the carrier frequency. This size dependence is captured by the difference between the two values of k_z where the spectral plane intersects the dispersion surface [Fig. 1(c)]. These points are given by k_0 and Eq. (3) (see Sec. A of the Supplemental Material [14]),

$$k_z' = \frac{2m\tan(\theta)}{\hbar} - k_0. \tag{3}$$

With $\theta \geqslant \arctan(\hbar k_0/m)$ so all the spectral components have $k_z > 0$, constrained to be only a forward propagating electron wave.

The colormap on Fig. 2(a) depicts the different sizes of the momentum space surface for different values of the group velocity, v_g, and the carrier wave number, k_0. For higher values of k_0, the lower v_g have a negative longitudinal spectral linewidth $k_{zd} = k_z' - k_0$, simply due to the fact that the point of intersection defined in the spectral plane, k_0, will be the maximum instead of the minimum. This is the region of subluminal electrons, where the group velocity falls below the group velocity at (k_0, ω_0) in Fig. 1(c). For higher k_0, it will also be increasingly difficult to construct a momentum space skyrmion before reaching the topological phase transition into a momentum space meron, despite higher-energy electrons should also be treated relativistically.

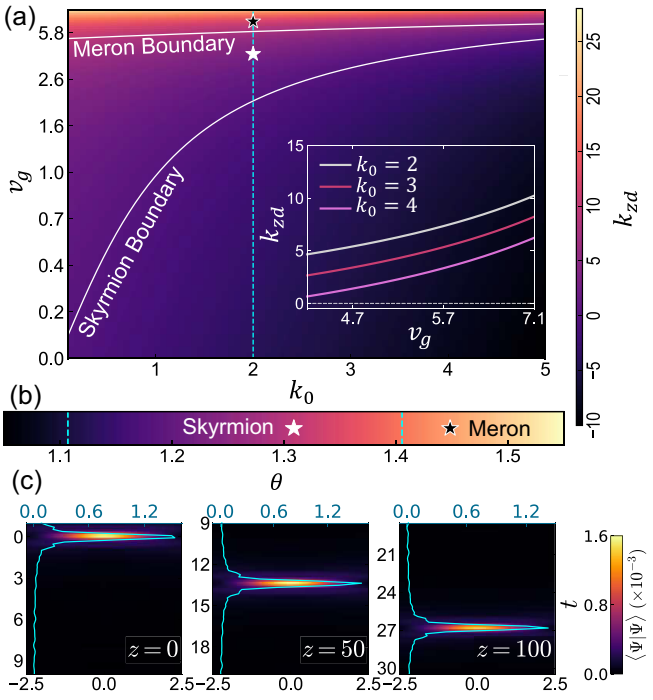


FIG. 2. (a) The allowed parameter space in v_g, k_0 to host skyrmion and meron in momentum space in an electron STWP. The colormap is the longitudinal spectral linewidth in momentum space, and the white and black stars are the points used for skyrmion and meron real-space calculations, respectively. Inset: The longitudinal spectral linewidth as a function of group velocity and carrier wave numbers. The shown k_{zd} is measured without a limit $k_{z\max}$. (b) The group velocity regions for a carrier wave number of $k_0 = 2$, shown using the spectral tilt angle. (c) The propagation invariance of the electron STWP can be seen by the almost unchanged peak intensity (blue line and axis) as the pulse moves from $z = 0$ to $z = 100$. The probability amplitude plot is scaled by 10^3 for clarity, and shown in the laboratory frame.

Within the regime where a skyrmion can be hosted, a higher k_0 with a fixed v_g gives a lower size of the skyrmion in momentum space [Fig. 2(a), inset], which directly impacts the spectral requirement of the electron plane waves required to synthesize the whole single electron wave packet. In reality, this difference in the spectral extent in the synthesis of the STWP is directly observable on the probability distribution in real space. Keeping $k_0 = 2.0$, the group velocity was tuned to construct the different momentum space surfaces and prove the boundaries given by the analytical derivations. The white stars are the parameters used to construct the skyrmion and the black stars are the parameters for the meron. Figure 2(b) shows the spectral tilt angle used instead of the group velocity for clarity.

Constructing the electron wavefunction with the allowed (k_x, k_y, ω) plane wave components on the momentum space surface is enough to create a propagation-invariant and nondiffracting electron STWP [see Fig. 2(c), the blue line and axes are the intensity at $x = 0$ overlaid onto the probability amplitude plot]. However, such a scalar STWP construction lacks a vector structure on the momentum space surface. Therefore, we detail now how the momentum space skyrmions and merons are constructed. We use the nonrelativistic electron spinor and impose it onto each point on the surface in momentum space. Effectively, this forms a momentum space skyrmion (similar to a momentum space meron in Ref. [33]) and in real space, it forms a propagating localized electron wave packet made up of momentum-spinor coupled plane waves.

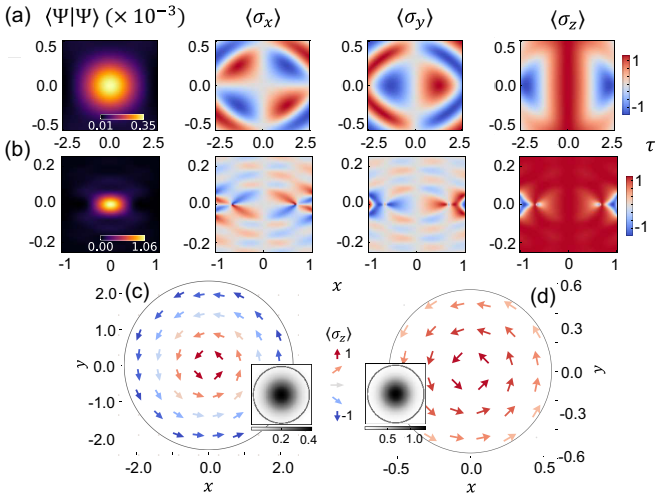


FIG. 3. The real-space structure of the electron wavefunction. (a), (b) The spatiotemporal structure for skyrmions and meron SEV, respectively, in the comoving frame. The SEV is normalized by the local probability amplitude. (c) The real-space SEV of the skyrmions and (d) merons. The in-plane arrows are directions of $\langle\sigma_x\rangle$ and $\langle\sigma_y\rangle$, while the colormap and legend gives the direction of $\langle\sigma_z\rangle$. Inset: Probability map of the electron pulse with the skyrmion and meron structure embedded, scaled to 10^3.

The spinor is defined as a two-component orthogonal state as in Eq. (4), which leads to the vectors on a Bloch sphere being defined as $\overline{n} = [\sin\theta\cos\phi,\ \sin\theta\sin\phi,\ \cos\theta]$. Here, m, γ are the vorticity and the helicity of the topological texture. In this paper, m, γ are set to 1 and 0, respectively. We adopt a polarity of 1 for the momentum space skyrmions and polarity of -1 for the momentum space merons (see Sec. C of the Supplemental Material [14]),

$$\chi = [\cos(\theta/2),\, e^{i(m\phi+\gamma)}\sin(\theta/2)]. \tag{4}$$

As the electron spin is an intrinsic quantity, we investigate the local SEV of the electron wavefunction in real space, given by $\langle\Psi|\boldsymbol{\sigma}|\Psi\rangle$, with Ψ being the real-space wavefunction $\Psi = \int A e^{i(k_x x + k_y y + k_z z - \omega t)}\chi(k_x, k_y)dk_x dk_y$. $\boldsymbol{\sigma}$ is the three-component Pauli matrices, A is the amplitude of each constituent plane wave from each point on the momentum space surface, and $\Psi = (\Psi_\uparrow, \Psi_\downarrow)$ is a two-component normalized wavefunction corresponding to the components of χ. The governing equation for Ψ should ideally be the Pauli equation, but with the absence of magnetic field, this is a two-component field satisfying independent Schrodinger equations. We define the vector $\mathbf{S} = (\langle\sigma_x\rangle, \langle\sigma_y\rangle, \langle\sigma_z\rangle)$, which is the local normalized SEV [Eq. (5)], and we note that this information is carried within each single electron wavefunction,

$$\mathbf{S} = \frac{\Psi^\dagger\boldsymbol{\sigma}\Psi}{\Psi^\dagger\Psi} = \frac{1}{\rho}\begin{pmatrix} 2\ \mathrm{Re}\left(\Psi_\uparrow^*\Psi_\downarrow\right) \\ 2\ \mathrm{Im}\left(\Psi_\uparrow^*\Psi_\downarrow\right) \\ |\Psi_\uparrow|^2 - |\Psi_\downarrow|^2 \end{pmatrix}, \tag{5}$$

where $\rho = |\Psi_\uparrow|^2 + |\Psi_\downarrow|^2$.

The construction of the skyrmions and merons was done in momentum space, while Eq. (5) was used to investigate the real-space probability distribution. Turning now to the behavior in real space, we projected the expectation values of the three Pauli matrices onto the $x - \tau$ plane [Figs. 3(a) and 3(b) for skyrmions and merons, respectively]. For skyrmion SEV, the radial transition from red to blue indicates a reversal of the out of plane component in $\langle\Psi|\sigma_z|\Psi\rangle$, and pole-to-pole coverage of the Bloch sphere. In contrast, the meron SEV do not exhibit pole-to-pole coverage.

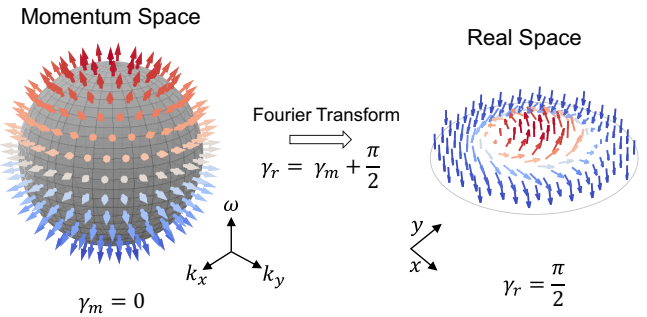


FIG. 4. The relation between the 3D Skyrmionic spinor texture in momentum space and its in-plane Fourier transformed counterpart in real space. There is a helicity shift of $\pi/2$ due to an extra i^m term, with $m = 1$ being the winding number (see Sec. B of the Supplemental Material [14]). γ_m is the helicity in momentum space of the spinor texture and γ_r is the real-space helicity.

Next, we plotted the SEV on the x–y plane ($z, t = 0$) [Figs. 3(c) and 3(d) for skyrmion and meron SEV, respectively]. For skyrmions, the center of the wave packet is oriented purely in the positive z direction ($\langle\sigma_z\rangle = 1$), and the ends of the high probability region has the expectation value of $\langle\sigma_z\rangle = -1$. For merons, the ends of the high probability region instead give $\langle\sigma_z\rangle = 0$. Interestingly, the textures were found to exhibit a $\pi/2$ phase shift in the helicity [Figs. 3(c) and 3(d)]. A Néel skyrmion in momentum space gives a Bloch SEV in real space, and the reason for this is an extra factor of i. Intuitively, the momentum space factor $e^{im\phi_k}$ is mapped to $i^m e^{im\phi}$ in real space. Hence, the integer winding m and the topological character of the texture, through the skyrmion number, is preserved, but the additional phase i^m rotates the in-plane spin orientation by $m\pi/2$. This accounts for the observed helicity shift for $m = 1$ (Fig. 4). The Fourier transform therefore reshapes the radial profile through the Bessel function (see Sec. B of the Supplemental Material for further details [14]). The existence of the skyrmion and meron local SEV permits the calculation of the skyrmion number in real space [Eq. (6)], which uses information encoded within each single electron wavefunction,

$$Q = \frac{1}{4\pi}\iint \mathbf{m}\cdot\left(\frac{\partial \mathbf{m}}{\partial x}\times\frac{\partial \mathbf{m}}{\partial y}\right)dx\,dy, \tag{6}$$

where $\mathbf{m}$ is the vector creating the texture. As the electron STWP adheres to the linear relation of k_z and ω [Figs. 1(c) and 1(f)], the matter wave packet is propagation invariant for large distances. It is therefore of interest to measure the propagation invariance of the skyrmion number in real space, and this is shown in Fig. 5 for skyrmions. The propagation invariance was measured in two

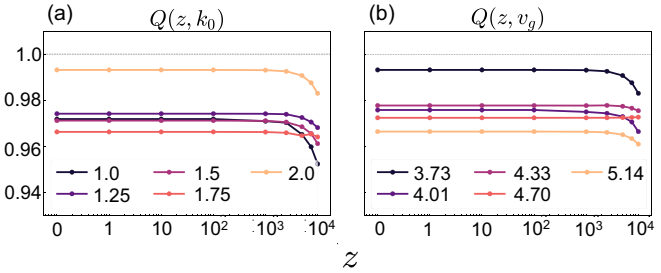


FIG. 5. (a) The propagation invariance of the skyrmion SEV for group velocity of $v_g = 3.73$ for different carrier wave numbers, and (b) the propagation invariance of the skyrmion SEV as a function of the group velocity, for $k_0 = 2.0$.

ways. First, by changing the carrier frequency and wave number, and second, by tuning the group velocity. Figure 5 shows both the measurements. Importantly, all the skyrmions propagate invariantly for large distances (10^3) before any large decays happen, which directly demonstrates that the tunable structures embedded within an electron STWP are propagation invariant for relatively long distances. The difference between the different decays at large distances for different group velocities and carrier wave number is due to the finite spectral weights. An ideal STWP will show a perfectly flat profile across all distances. The space-time meron textures were already produced recently in optical STWP [33], which inherits the propagation invariance automatically from the STWP construction as well.

In experiments, recent progress in electron wave shaping [1–3,5,6] may be used to sculpt the spatiotemporal spectrum of the electron wave packet. To imprint spinor textures onto a free-electron plane waves in momentum space, a magnetic field may be utilized to give a probability distribution and realize the full or half Bloch sphere. This work is a general property of the quadratic dependence of the frequency on the momentum in the free-electron dispersion relation. For other waves, the pseudospin degree of freedom intrinsic to quasiparticles may also be used [50,51].

III. CONCLUSION

In summary, we demonstrate that free-space propagating STWPs can be created using nonrelativistic free-electron matter waves, and the electron spinor can be used to construct propagation-invariant momentum space topological textures tunable by the group velocity and the carrier wave number. At high group velocities, the momentum space surface will only host merons, as there is no closed momentum space surface directly obtained through the intersection of the spectral plane and the dispersion surface. However, at lower group velocities, the parabolic nature of the free-electron dispersion naturally allows a closed sphere in (k_x, k_y, ω) space. The closed momentum space structure allows the construction of momentum space skyrmions and forms an analogous Bloch sphere.

By this particular tuning, we show the possibility to generate persistent skyrmionic SEV structures in real space that exhibit a helicity phase shift of $\pi/2$.

This paper reveals a new class of free-space wave packet with a topological wavefunction and charge, whose topology is independently tunable without material band structures. As this topological information exists in real space, this may be a new robust route to transporting information with matter and for sensing applications.

Another property automatically inherited from the space-time wave packets structure is self healing [52], which allows the skyrmions and meron SEV proposed here to propagate for large distances even with small perturbations. This approach provides a bridge between STWP and structured matter waves, and the proposed system may also offer a platform for studying tunable topological textures in matter waves beyond conventional methods typically done through Bose-Einstein condensates [53–57]. To the best of our knowledge, this is the first single electron wave packet free-space propagating skyrmion, shown via the local SEV of electrons, and we assert this is still a single electron state. Our work opens up a range of possibilities of integration with a large body of existing literature on optical skyrmions and free-electron behavior. Such electron skyrmionic wave packets may be relevant to free-electron quantum optics, free-electron-photon interactions, may provide additional degrees of freedom for free-electron entanglement, microscopy, free-electron-matter interaction, and transition radiation and light generation by free electrons [58–64], as well as any future schemes for information encoding and transfer that will empower future technologies.

ACKNOWLEDGMENTS

Singapore Ministry of Education (MOE) AcRF Tier 1 (RG157/23 & RT11/23), Singapore Agency for Science, Technology and Research (A*STAR) (M24N7c0080 & H25-MRO3489), and Nanyang Assistant Professorship Start Up grant.

DATA AVAILABILITY

The numerical simulations that support the findings of this study are openly available [65].

[1] B. J. McMorran, A. Agrawal, I. M. Anderson, A. A. Herzing, H. J. Lezec, J. J. McClelland, and J. Unguris, Electron vortex beams with high quanta of orbital angular momentum, Science **331**, 192 (2011).

[2] S. Lloyd, M. Babiker, G. Thirunavukkarasu, and J. Yuan, Electron vortices: Beams with orbital angular momentum, Rev. Mod. Phys. **89**, 035004 (2017).

[3] Y. Fang, J. Kuttruff, D. Nabben, and P. Baum, Structured electrons with chiral mass and charge, Science **385**, 183 (2024).

[4] Y. Fang, J. Kuttruff, and P. Baum, Electron matter waves with internal torque, Nat. Phys. **22**, 838 (2026).

[5] I. Madan, V. Leccese, A. Mazur, F. Barantani, T. LaGrange, A. Sapozhnik, P. M. Tengdin, S. Gargiulo, E. Rotunno, J.-C. Olaya, *et al.*, Ultrafast transverse modulation of free electrons by interaction with shaped optical fields, ACS Photon. **9**, 3215 (2022).

[6] O. Reinhardt and I. Kaminer, Theory of shaping electron wavepackets with light, ACS Photon. **7**, 2859 (2020).

[7] S. R. Greig, J. B. Khurgin, and A. Y. Elezzabi, Nonrelativistic electron–electron Møller scattering in a nonadiabatic tunnel-ionizing surface plasmon field, Commun. Phys. **3**, 28 (2020).

[8] A. Gliserin, M. Walbran, F. Krausz, and P. Baum, Sub-phonon-period compression of electron pulses for atomic diffraction, Nat. Commun. **6**, 8723 (2015).

[9] C. D. Arrowsmith, K. G. Miller, M. V. Ambat, S.-W. Bahk, I. A. Begishev, J. Bromage, S. Bucht, N. Dauphin, C. Dorrer, C. Jeon, *et al.*, Dephasingless laser wakefield acceleration of electrons using a flying focus, Nat. Phys. **22**, 1513 (2026).

[10] F. Pennacchio, G. M. Vanacore, G. F. Mancini, M. Oppermann, R. Jayaraman, P. Musumeci, P. Baum, and F. Carbone, Design and implementation of an optimal laser pulse front tilting scheme for ultrafast electron diffraction in reflection geometry with high temporal resolution, Struct. Dyn. **4**, 044032 (2017).

[11] Y. Wang and C.-F. Li, Bessel-Gaussian electron beams of cylindrically symmetric spin polarization, Europhys. Lett. **95**, 44001 (2011).

[12] K. Denisov, I. Rozhansky, N. Averkiev, and E. Lähderanta, Electron scattering on a magnetic skyrmion in the nonadiabatic approximation, Phys. Rev. Lett. **117**, 027202 (2016).

[13] H. Swain, A. Mandal, S. Satpathy, and B. R. K. Nanda, Quantum dynamics of electron scattering from skyrmions, Phys. Rev. B **113**, 104446 (2026).

[14] See Supplemental Material at http://link.aps.org/supplemental/10.1103/pnvl-7bx7 for details on the scattering simulations, derivations of the longitudinal spectral linewidth and derivations of the $\pi/2$ helicity phase shift.

[15] L. A. Hall and A. F. Abouraddy, Spectral reorganization of space-time wave packets in the presence of normal group-velocity dispersion, Phys. Rev. A **111**, 063515 (2025).

[16] D. Kim, C. Guo, P. B. Catrysse, and S. Fan, Shaping space-time wave packets beyond the paraxial limit using a dispersion magnifier, Phys. Rev. A **111**, 013504 (2025).

[17] H. E. Kondakci and A. F. Abouraddy, Diffraction-free pulsed optical beams via space-time correlations, Opt. Express **24**, 28659 (2016).

[18] H. E. Kondakci and A. F. Abouraddy, Optical space-time wave packets having arbitrary group velocities in free space, Nat. Commun. **10**, 929 (2019).

[19] M. A. Romer, L. A. Hall, and A. F. Abouraddy, Synthesis and characterization of space-time light sheets: A tutorial, J. Opt. **27**, 013501 (2025).

[20] X. Su, K. Zou, Y. Wang, M. Yessenov, H. Zhou, H. Song, W. Ko, R. Zeng, A. Alhaddad, M. Ramakrishnan, Y. Duan, A. F. Abouraddy, M. Tur, D. N. Christodoulides, and A. E. Willner, Space-time wave packets in multimode optical fibers with controlled dynamic motions and tunable group velocities, Nat. Commun. **16**, 2027 (2025).

[21] H. Wang, C. Guo, and S. Fan, Spatiotemporal steering of nondiffracting wave packets, Phys. Rev. Lett. **134**, 073803 (2025).
[22] M. Yessenov and A. F. Abouraddy, Accelerating and decelerating space-time optical wave packets in free space, Phys. Rev. Lett. **125**, 233901 (2020).
[23] M. Yessenov, L. A. Hall, K. L. Schepler, and A. F. Abouraddy, Space-time wave packets, Adv. Opt. Photon. **14**, 455 (2022).
[24] M. Yessenov, J. Free, Z. Chen, E. G. Johnson, M. P. J. Lavery, M. A. Alonso, and A. F. Abouraddy, Space-time wave packets localized in all dimensions, Nat. Commun. **13**, 4573 (2022).
[25] H. E. Kondakci and A. F. Abouraddy, Diffraction-free space–time light sheets, Nat. Photon. **11**, 733 (2017).
[26] Q. Zhan, Spatiotemporal sculpturing of light: A tutorial, Adv. Opt. Photon. **16**, 163 (2024).
[27] Z. Che, W. Liu, J. Ye, L. Shi, C. Chan, and J. Zi, Generation of spatiotemporal vortex pulses by resonant diffractive grating, Phys. Rev. Lett. **132**, 044001 (2024).
[28] S. Liu, H. Ge, X.-Y. Xu, Y. Sun, X.-P. Liu, M.-H. Lu, and Y.-F. Chen, Generation of spatiotemporal acoustic vortices with arbitrarily oriented orbital angular momentum, Nat. Commun. **16**, 2823 (2025).
[29] A. Pitanti, N. Ashurbekov, I. dePedro Embid, M. Msall, and P. V. Santos, GHz acousto-optic angular momentum with tunable topological charge, Nat. Commun. **16**, 8116 (2025).
[30] A. Singh, J. Rønning, C.-C. Liu, L. Angheluta, A. Concha, and M. M. Bandi, Topology made visible through standing waves in a spinning fluid, Commun. Phys. **9**, 123 (2026).
[31] D. A. Smirnova, F. Nori, and K. Y. Bliokh, Water-wave vortices and skyrmions, Phys. Rev. Lett. **132**, 054003 (2024).
[32] H. Zhang, Y. Sun, J. Huang, B. Wu, Z. Yang, K. Y. Bliokh, and Z. Ruan, Topologically crafted spatiotemporal vortices in acoustics, Nat. Commun. **14**, 6238 (2023).
[33] M. Yessenov, A. H. Dorrah, C. Guo, L. A. Hall, J.-S. Park, J. Free, E. G. Johnson, F. Capasso, S. Fan, and A. F. Abouraddy, Ultrafast space-time optical merons in momentum-energy space, Nat. Commun. **16**, 8592 (2025).
[34] C. Guo, M. Xiao, Y. Guo, L. Yuan, and S. Fan, Meron spin textures in momentum space, Phys. Rev. Lett. **124**, 106103 (2020).
[35] C. Guo, M. Xiao, M. Orenstein, and S. Fan, Structured 3D linear space–time light bullets by nonlocal nanophotonics, Light Sci. Appl. **10**, 160 (2021).
[36] T. Skyrme, A unified field theory of mesons and baryons, Nucl. Phys. **31**, 556 (1962).
[37] Y. Shen, H. Wang, and S. Fan, Free-space topological optical textures: Tutorial, Adv. Opt. Photon. **17**, 295 (2025).
[38] C. Psaroudaki and C. Panagopoulos, Skyrmion qubits: A new class of quantum logic elements based on nanoscale magnetization, Phys. Rev. Lett. **127**, 067201 (2021).
[39] Y. Shen, Q. Zhang, P. Shi, L. Du, X. Yuan, and A. V. Zayats, Optical skyrmions and other topological quasiparticles of light, Nat. Photon. **18**, 15 (2024).
[40] H. Teng, X. Liu, N. Zhang, H. Fan, G. Chen, Q. Cao, J. Zhong, X. Lei, and Q. Zhan, Construction of optical spatiotemporal skyrmions, Light Sci. Appl. **14**, 324 (2025).
[41] L. Niu, X. Feng, X. Zhang, W. Yu, Q. Wang, Y. Lang, Q. Xu, X. Chen, J. Ma, H. Qiu, Y. Shen, W. Zhang, and J. Han, Electric-magnetic-switchable free-space skyrmions in toroidal light pulses via a nonlinear metasurface, Optica **13**, 203 (2026).
[42] Y. Shen, Y. Hou, N. Papasimakis, and N. I. Zheludev, Supertoroidal light pulses as electromagnetic skyrmions propagating in free space, Nat. Commun. **12**, 5891 (2021).
[43] R. Wang, B. Ying, S. Shi, J. Wang, B.-Z. Wang, M. Liang, and Y. Shen, Hybrid electromagnetic toroidal vortices, Sci. Adv. **11**, eads4797 (2025).
[44] A. Zdagkas, C. McDonnell, J. Deng, Y. Shen, G. Li, T. Ellenbogen, N. Papasimakis, and N. I. Zheludev, Observation of toroidal pulses of light, Nat. Photon. **16**, 523 (2022).
[45] Y. Shen, N. Papasimakis, and N. I. Zheludev, Nondiffracting supertoroidal pulses and optical "Kármán vortex streets", Nat. Commun. **15**, 4863 (2024).

[46] R. Wang, P.-Y. Bao, Z.-Q. Hu, S. Shi, B.-Z. Wang, N. I. Zheludev, and Y. Shen, Observation of resilient propagation and free-space skyrmions in toroidal electromagnetic pulses, Appl. Phys. Rev. **11**, 031411 (2024).
[47] A. A. Wang, Z. Zhao, Y. Ma, Y. Cai, R. Zhang, X. Shang, Y. Zhang, J. Qin, Z.-K. Pong, T. Marozsák, B. Chen, H. He, L. Luo, M. J. Booth, S. J. Elston, S. M. Morris, and C. He, Topological protection of optical skyrmions through complex media, Light Sci. Appl. **13**, 314 (2024).
[48] Z. Guo, C. Peters, N. Mata-Cervera, A. N. Vetlugin, R. Guo, P. Zhang, A. Forbes, and Y. Shen, Topological robustness of classical and quantum optical skyrmions in atmospheric turbulence, Nat. Commun. **17**, 2085 (2026).
[49] Y. Zhang, A. A. Wang, R. Zhang, Z. Zhao, Y. Ma, R. Liu, Z.-K. Pong, Y. Cai, and C. He, Skyrmions based on optical anisotropy for topological encoding, Light Sci. Appl. **15**, 254 (2026).
[50] Y. He, G. Luo, H. Sohn, O. Matsuda, O. B. Wright, and Z. Su, Revealing intrinsic 3D spin angular momentum of evanescent acoustic phonons on a single-crystal surface using ultrafast optoacoustics, Nat. Commun. **17**, 3520 (2026).
[51] C. Herring and C. Kittel, On the theory of spin waves in ferromagnetic media, Phys. Rev. **81**, 869 (1951).
[52] H. E. Kondakci and A. F. Abouraddy, Self-healing of space-time light sheets, Opt. Lett. **43**, 3830 (2018).
[53] U. Al Khawaja and H. Stoof, Skyrmions in a ferromagnetic Bose–Einstein condensate, Nature (London) **411**, 918 (2001).
[54] T.-L. Ho, Spinor Bose condensates in optical traps, Phys. Rev. Lett. **81**, 742 (1998).
[55] L. S. Leslie, A. Hansen, K. C. Wright, B. M. Deutsch, and N. P. Bigelow, Creation and detection of skyrmions in a Bose-Einstein condensate, Phys. Rev. Lett. **103**, 250401 (2009).
[56] K.-P. Marzlin, W. Zhang, and B. C. Sanders, Creation of skyrmions in a spinor Bose-Einstein condensate, Phys. Rev. A **62**, 013602 (2000).
[57] J. Ruostekoski and J. R. Anglin, Creating vortex rings and three-dimensional skyrmions in Bose-Einstein condensates, Phys. Rev. Lett. **86**, 3934 (2001).
[58] S. Tsesses, G. Bartal, and I. Kaminer, Light generation via quantum interaction of electrons with periodic nanostructures, Phys. Rev. A **95**, 013832 (2017).
[59] I. D. Feranchuk and A. Ulyanenkov, Transition radiation from electrons: Application to thin film and superlattice analysis, Phys. Rev. B **63**, 155318 (2001).
[60] A. Konečná, F. Iyikanat, and F. J. García de Abajo, Entangling free electrons and optical excitations, Sci. Adv. **8**, eabo7853 (2022).
[61] R. Ruimy, A. Karnieli, and I. Kaminer, Free-electron quantum optics, Nat. Phys. **21**, 193 (2025).
[62] G. Baranes, R. Ruimy, A. Gorlach, and I. Kaminer, Free electrons can induce entanglement between photons, npj Quantum Inf. **8**, 32 (2022).
[63] Z. Xie, Z. Chen, H. Li, Q. Yan, H. Chen, X. Lin, I. Kaminer, O. D. Miller, and Y. Yang, Maximal quantum interaction between free electrons and photons, Phys. Rev. Lett. **134**, 043803 (2025).
[64] D. N. Makarov, K. A. Makarova, S. N. Kapustin, A. A. Goshev, and Y. V. Tsykareva, Quantum entanglement of non-monochromatic photons on free electrons, J. Opt. Soc. Am. B **42**, 189 (2025).
[65] https://doi.org/10.21979/N9/EFUNNW.